Surface Roughness and Spectral Analysis Using Airborne Lidar Digital Elevation Models (DEMs) for Modeling and Calibration/Validation of GNSS-R Land Returns

Tianlin Wang[(1)], Joel T. Johnson[(1)], Alexandra Bringer[(2)], Yuchan Yi[(1)], and Mohammad Al-Khaldi[(1)]
(1) The Ohio State University, Columbus, OH USA; e-mail: wang.15085@osu.edu;
johnson.1374@osu.edu; yi.3@osu.edu; al-khaldi.2@osu.edu
(2) NASA Goddard Space Flight Center, Greenbelt, MD USA; e-mail: alexandra.m.bringer@nasa.gov

Abstract

Surface roughness serves as one of key inputs to traditional scattering models to predict bistatic scattered fields; these model predictions can then be used to support the calibration and/or validation of GNSS-R land observations. Lidar datasets over the San Luis Valley and the vicinity of White Sands were acquired in two airborne campaigns to provide information on surface properties for this application, including non-detrended and detrended root mean square (rms) height, mean slopes, and the variance of slopes over a fixed patch size of 30 meters. A spectral analysis of surface roughness using the power spectral density (PSD) was also conducted. The 2-D PSD shows the different characteristics of 'flat' and 'rough' surfaces. A normalized 1-D PSD derived by averaging 2-D results over azimuth. A parameterization method is proposed to describe this 1-D spectrum using a power law function with an exponent and a scale length. The parameterized spectrum can be applied in further studies of scattering models and the cal/val of GNSS-R land returns.

1 Introduction

Interest in GNSS-Reflectometry has significantly grown following the launch of TechDemoSat-1 [1] in 2014 and NASA's Cyclone Global Navigation Satellite System (CYGNSS) [2] mission in 2016. Analysis of datasets from the two missions has revealed the presence of coherent reflected signals over land and thus motivated multiple investigations focused on modeling the near specular reflection of GNSS signals from Earth's land surface [3-8].

To model scattering fields and calibrate GNSS-R land returns, traditional scattering theories require knowledge of the geometry, the frequency of operation, and a description of the land surface roughness. Existing topographic digital elevation models (DEMs), such as the SRTM standard 30-m product [9], are used to infer surface roughness information. However, these products' coarse spatial resolution and meter-scale vertical uncertainties make it impossible to reveal the 'intermediate' scale roughness using existing DEMs alone. In contrast, airborne lidar measurements can provide finer spatial resolutions and higher vertical accuracies over low vegetation areas.

Two areas (in the San Luis Valley, CO and in the vicinity of the White Sands, NM) have been selected as CYGNSS land calibration/validation (cal/val) sites and instrumented with Soil Moisture Sensing Controller And oPtimal Estimator (SoilSCAPE) wireless sensor networks [10]. As given in Figure 1, an analysis of CYGNSS returns over the two areas shows that: 1) The complex topography of the San Luis Valley may create coherent returns in some situations, however, they are not consistently repeated as the coherent recurrence stays below 50% over most of the area; 2) The coherent returns in the White Sands area are more consistently repeated, and very high coherent recurrence appears in the southern part of the area [11, 12].
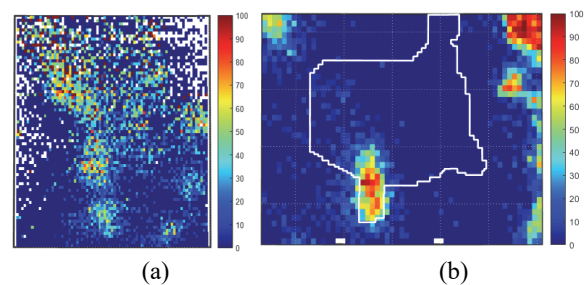

Figure 1. Coherence recurrence map computed from CYGNSS mission observations for (a) San Luis Valley site (b) White Sands site.

To support CYGNSS land cal/val activities, airborne Lidar measurements were acquired by Survey And Mapping, Inc. (SAM) over the two areas. The lidar data consists of full waveform data, point cloud data, a DEM at 30 cm grid resolution, and a DEM at 10 cm grid resolution interpolated from the 30 cm DEM. The waveforms represent the lowest-level data product, while point clouds contain 4D-position/time, intensity, scan angle, etc., and the DEM is the highest-level data product.
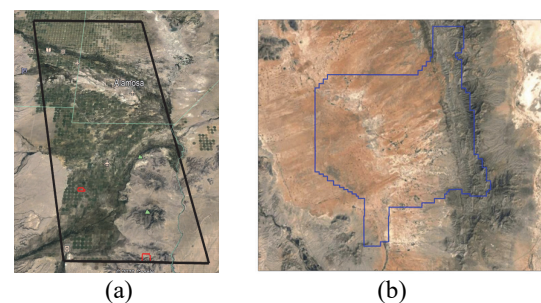

Figure 2. Lidar survey area of (a) San Luis Valley site; (b) White Sands site.

2 Surface Roughness

Areas within the 30 cm resolution lidar DEM were first sub-divided into "patches" of a specified horizontal size, e.g. 30 m. The surface roughness properties, including the root mean square (rms) height, mean slope, and variance of slopes were then computed for each patch. Examples of the DEM, rms height, detrended rms height of the White Sands area at 30 m resolution are shown in Figure 3. It is noted that the southern part of the survey area has the lowest rms height, mean slope, and variance slope, which corresponds to the area with highest recurrence of coherent reflections [13].
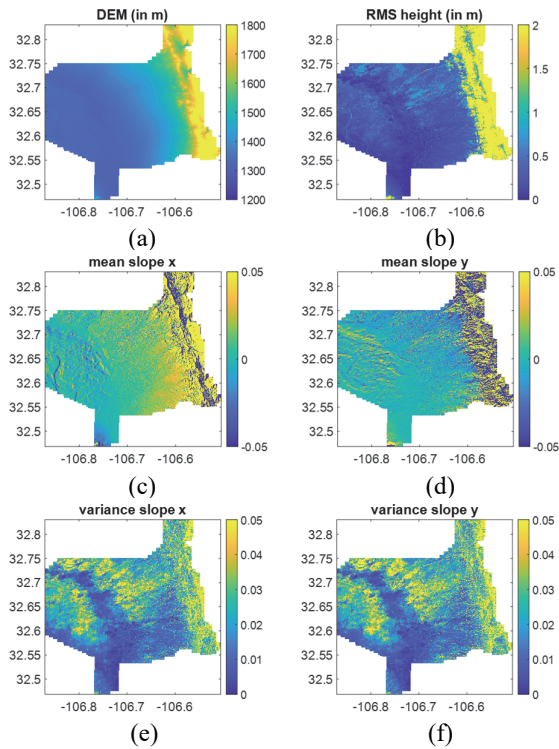

(a) (b)

(c) (d)

(e) (f)

Figure 3. White Sands site: (a) DEM, (b) rms height, (c) mean slope East, (b) mean slope North, (e) variance slope East, (f) variance slope North

The patches were also detrended by subtracting a best-fit plane from the raw data for each 30 m patch, and the rms height of the detrended surface obtained, as shown in Figure 4.
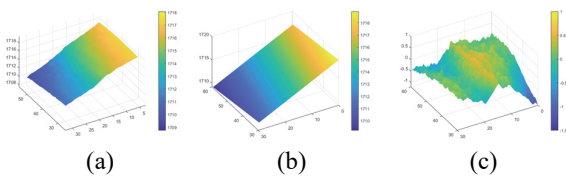

(a) (b) (c)

Figure 4. Detending a 30 m by 30 m patch: (a) raw DEM, (b) best-fit plane, (c) detrended DEM

The computed rms height map using the detrended DEMs is shown in Figure 5. Compared with the non-detrended rms height in Figure 3(b), the detrending process minimizes the effect of topographic variations.
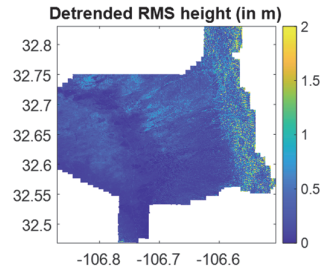

Figure 5. Detrended rms height of the White Sands site

The surface roughness properties for San Luis Valley and White Sands sites are being made available to the public on the NASA/JPL Physical Oceanography Distributed Active Archive Center (PO.DAAC).

3 Spectral Analysis

3.1 2-D Power Spectral Density

The power spectral density (PSD) decomposes surface roughness into contributions from different spatial frequencies [14, 15]. The 2-D PSD for a given surface patch can be computed by taking the amplitude squared of the 2-D FFT of the surface roughness [16, 17].

Examples of 30 m patches and the calculated PSD are shown in Figure 6. It is noticed that surface structure affects both the absolute power and directional spreading of PSD: the relatively flat surface has a smaller absolute power and less variability over the azimuth; while the rougher surface has much larger absolute power and more azimuthal spreading.
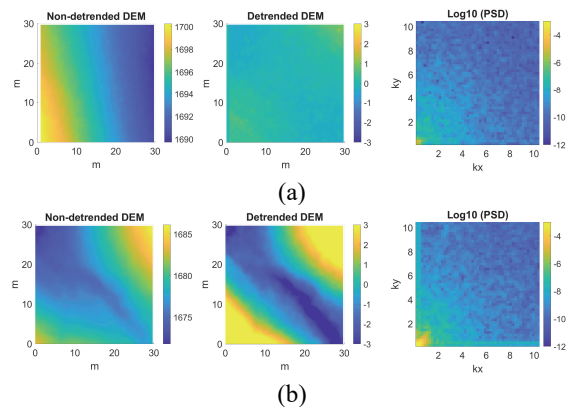

(a)

(b)

Figure 6. Examples of 2-D PSD calcualtion: (a). relatively flat surface; (b) rough surface. Left plots: non-detrended patch DEM, middle plots: detrended DEM, right plot: 2-D PSD using a logarithmic amplitude scale (zero wavenumber at leftmost corner)

3.2 1-D PSD vs. Patch Size

The 2-D PSD $W(k_x, k_y)$ can averaged over the azimuth to obtain a 1-D PSD

$$W(k) = \frac{1}{N} \sum_{i=1}^{N} W(k_x, k_y) \qquad (1)$$

where N denotes the number of azimuthal cuts.

The 1-D PSD can further by divided by its peak value to obtain a normalized PSD $W_N(k)$

$$W_N(k) = \frac{W(k)}{max[W(k)]} \qquad (2)$$

A DEM near the Jornada cal/val site JR-1, as shown in Figure 7(a), was selected to demonstrate the PSD calculation. The normalized 1-D PSDs for different patch sizes at 30m, 90m, and 180m were then computed and are plotted in Figure 7(b). It is noted that the high-frequency parts of the spectrum from three cases are close to each other, while the low-frequency part varies as should be expected for increasing patch dimensions. The consistent apparent power law behavior at large wavenumber in the three cases suggests that the high frequency portion of the spectrum remains stationary in this region of over length scales 30 to 180 m.
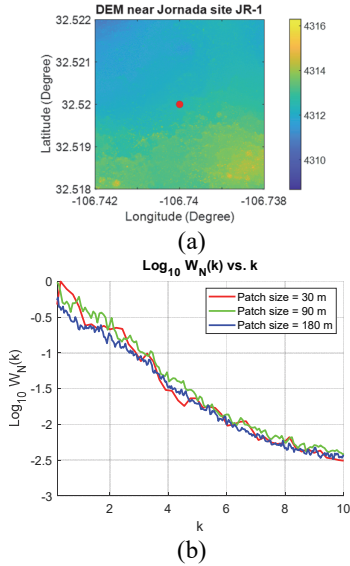

(a)

(b)

Figure 7. (a). Selected DEM near JR-1 site; (b) normalized 1-D PSD vs. wavenumber for different patch sizes

3.3 Parameterized Spectrum

The normalized 1-D PSD was calculated for all 30 m × 30 m patches and then fit with the functional form [18, 19]

$$W_{PL}(k) = (1 + k^2 L^2)^\gamma \qquad (3)$$

where the exponent γ is determined by fitting the slope (in log-space) using the high-frequency part of the spectrum, and the scale length L is determined by minimizing a cost function:

$$cost(L) = \sum_{k=0}^{k_c} [\log W_{PL}(k, \gamma, L) - \log W_N(k)]^2 \qquad (4)$$

where k_c is the cutoff wavenumber of the spectrum.

Preliminary results for the exponent γ and scale length L are shown in Figure 8. Note that the two parameters are dependent on the type of spectral function as well as the selected patch size and spatial resolution of the DEM. Further analyses are in progress with results to be reported at the presentation.
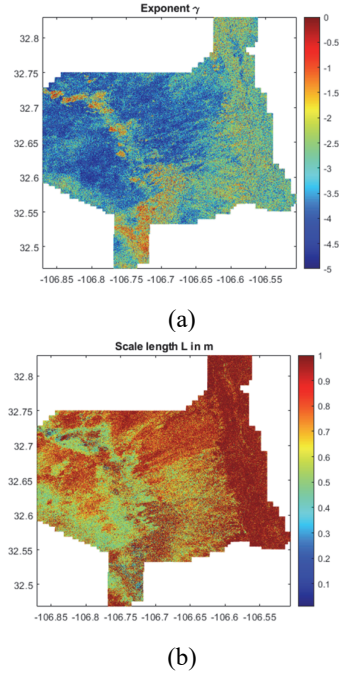

(a)

(b)

Figure 8. Parameterized surface spectrum for White Sands site: (a) exponent γ (b) scale length L (m)

4 Summary

Airborne lidar datasets are essential for assessing the presence of roughness on the "intermediate" $\sim 1 - 30$ m horizontal scales of surface topography. Surface roughness results from multiple airborne lidar campaigns and their spectral analysis were reported in this paper. The derived roughness properties and parameterized spectrum could serve as key inputs to electromagnetic wave scattering models and play a significant role in the cal/val of CYGNSS land data. In combination with the in-situ soil moisture measured by SoilScape sensors, these may be helpful for other GNSS and signal-of-opportunity reflectometry missions.

References

[1] Unwin, M., Duncan, S., Jales, P., Blunt, P. and Tye, J., "Implementing GNSS-reflectometry in Space on the TechDemoSat-1 Mission," Proceedings of the 27th International Technical Meeting of the Satellite Division of The Institute of Navigation (ION GNSS+ 2014), Tampa, Florida, Sept 2014, pp. 1222-1235.

[2] C. Ruf, D. McKague, D. Posselt, S. Gleason, M. P. Clarizia, V. Zavorotny, T. Butler, J. Redfern, W. Wells, M. Morris, J. Crespo, C. Chew, E. Small, D. Pasqual, T. Wang, A. Warnock, D. Mayers, M. Al-Khaldi and A. J. O'Brien, "Cyclone Global Navigation Satellite System," Michigan Publishing, University of Michigan, Ann Arbor, MI, 2022.

[3] A. M. Balakhder, M. M. Al-Khaldi and J. T. Johnson, "On the Coherency of Ocean and Land Surface Specular Scattering for GNSS-R and Signals of Opportunity Systems", IEEE Trans. Geosci. Remote Sens., vol. 57, no. 12, pp. 10426-10436, Sep. 2019.

[4] B. Ren, J. Zhu, L. G. Tsang and H. Xu, "Analytical Kirchhoff Solutions (AKS) and Numerical Kirchhoff Approach (NKA) for First-Principle Calculations of Coherent Waves and Incoherent Waves at P Band and L band in Signals of Opportunity (SoOP)", Prog. Electromagn. Res., vol. 171, pp. 35-73, 2021.

[5] D. Comite, F. Ticconi, L. Dente, L. Guerriero and N. Pierdicca, "Bistatic Coherent Scattering from Rough Soils with Application to GNSS Reflectometry", IEEE Trans. Geosci. Remote Sens., vol. 58, no. 1, pp. 612-625, Jan. 2020.

[6] L. Dente, L. Guerriero, D. Comite and N. Pierdicca, "Space-borne GNSS-R Signal Over a Complex Topography: Modeling and Validation", IEEE J. Sel. Topics Appl. Earth Observ. Remote Sens., vol. 13, pp. 1218-1233, 2020.

[7] J. D. Campbell, A. Melebari and M. Moghaddam, "Modeling the Effects of Topography on Delay-Doppler Maps", IEEE J. Sel. Topics Appl. Earth Observ. Remote Sens., vol. 13, pp. 1740-1751, 2020.

[8] J. Campbell, R. Akbar, A. Bringer, D. Comite, L. Dente, S. Gleason, L. Guerriero, E. Hodges, J. Johnson, S. Kim, A. Melebari, N. Pierdicca, C. Ruf, L. Tsang, T. Wang, H. Xu, J. Zhu, and M. Moghaddam, "Intercomparison of Electromagnetic Scattering Models for Delay-Doppler Maps Along a CYGNSS Land Track with Topography," IEEE Trans. Geosci. Remote Sens., vol. 60, pp. 1-13, 2022, Art no. 2007413.

[9] T.G. Farr, P.A. Rosen, E. Caro, R. Crippen, R. Duren, S. Hensley, M. Kobrick, M. Paller, E. Rodriguez, L. Roth, D. Seal, S. Shaffer, J. Shimada, J. Umland, M. Werner, M. Oskin, D. Burbank, and D.E. Alsdorf, "The Shuttle Radar Topography Mission," Reviews of Geophysics, v. 45, no. 2, RG2004, 2007.

[10] M. Moghaddam, D. Entekhabi, Y. Goykhman, K. Li, M. Liu, A. Mahajan, A. Nayyar, D. Shuman, and D. Teneketzis, "A Wireless Soil Moisture Smart Sensor Web Using Physics-Based Optimal Control: Concept and Initial Demonstrations," IEEE J. Sel. Topics Appl. Earth Observ. Remote Sens., vol. 3, no. 4, pp. 522-535, Dec. 2010.

[11] A. Bringer, T. Wang, and J. Johnson, "Analysis of Lidar Digital Elevation Models to Support CYGNSS Cal/Val Activities," 2022 Int. Geosci. Remote Sens. Symp., Kuala Lumpur, Malaysia, July 17-22, 2022.

[12] T. Wang, A. Bringer, and J. Johnson, "A Study of The Relationship Between Surface Roughness and GNSS-R Coherent Returns Over Land," 2022 Int. Geosci. Remote Sens. Symp., Kuala Lumpur, Malaysia, July 17-22, 2022.

[13] T. Wang, J. Johnson, A. Bringer, Y. Yi, and M. M. Al-Khaldi, "Derivation of Surface Properties from Airborne Lidar Digital Elevation Models to Support CYGNSS Land Cal/Val Activities," Submitted to the 2023 Int. Geosci. Remote Sens. Symp., under review.

[14] B. N. Persson, O. Albohr, U. Tartaglino, A. I. Volokitin, and E. Tosatti, "On the Nature of Surface Roughness with Application to Contact Mechanics, Sealing, Rubber Friction and Adhesion," Journal of Physics: Condensed Matter, vol. 17, no. 1, R1-R62, 2004.

[15] T. D. Jacobs, T. Junge, and L. Pastewka, "Quantitative Characterization of Surface Topography Using Spectral Analysis," Surface Topography: Metrology and Properties, vol. 5, no. 1, 013001, 2017.

[16] T. Schlömer and O. Deussen, "Accurate Spectral Analysis of Two-Dimensional Point Sets," Journal of Graphics, GPU, and Game Tools, vol. 15, no. 3, pp. 152-160, 2011.

[17] M. Gircys and B. J. Ross, "Image Evolution Using 2D Power Spectra," Complexity, vol. 2019, Article 7293193, 2019.

[18] Q. Li, J. Shi, and K. S. Chen, "A Generalized Power Law Spectrum and Its Applications to the Backscattering of Soil Surfaces Based on the Integral Equation Model," IEEE Trans. Geosci. Remote Sens., vol. 40, no. 2, pp. 271–280, Feb. 2002.

[19] A. Darawankul and J. T. Johnson, "Band-Limited Exponential Correlation Function for Rough-Surface Scattering," IEEE Trans. Geosci. Remote Sens., vol. 45, no. 5, pp. 1198-1206, May 2007.